

Complex Refractive Index of Titan's Aerosol Analogues in the 200–900 nm Domain

S. I. Ramirez

Laboratoire Interuniversitaire des Systèmes Atmosphériques, UMR 7583, Universités Paris 7 et Paris 12, Paris, France and Laboratorio de Química de Plasmas y Estudios Planetarios, Instituto de Ciencias Nucleares, Universidad Nacional Autónoma de México, México DF, México

E-mail: ramirez@lisa.univ-paris12.fr, sramirez@nuclecu.unam.mx

P. Coll

Laboratoire Interuniversitaire des Systèmes Atmosphériques, UMR 7583, Universités Paris 7 et Paris 12, Paris, France

A. da Silva

Laboratoire d'Optique des Solides, UMR 7601, Université Paris 6, Paris, France

R. Navarro-González

Laboratorio de Química de Plasmas y Estudios Planetarios, Instituto de Ciencias Nucleares, Universidad Nacional Autónoma de México, México DF, México

J. Lafait

Laboratoire d'Optique des Solides, UMR 7601, Université Paris 6, Paris, France

and

F. Raulin

Laboratoire Interuniversitaire des Systèmes Atmosphériques, UMR 7583, Universités Paris 7 et Paris 12, Paris, France

Received May 16, 2000; revised October 12, 2001

The main gas-phase constituents of Titan's upper atmosphere, N₂ and CH₄, are photolyzed and radiolyzed by solar photons and magnetospheric electrons, respectively. The primary products of these chemical interactions evolve to heavier organic compounds that are likely to associate into the particles of haze layers that hide Titan's surface. The different theories and models that have been put forward to explain the characteristics and properties of the haze composites require a knowledge of their optical properties, which are determined by the complex refractive index. We present a new set of values for refractive index n and extinction coefficient k calculated directly from the transmittance and reflectance curves exhibited by a laboratory analogue of Titan's aerosols in the 200–900 nm range. Improvements in the aerosol analogue quality have been made. The effects of variables such as the uncertainty in sample thickness, aerosol porosity, and amount of scattered light on the final n and k values are assessed and discussed. Within the studied wavelength domain, n varies from 1.53 to 1.68 and k varies from 2.62×10^{-4} to 2.87×10^{-2} . These final n and k values should be considered as a new reference to modelers who compute the properties of Titan's aerosols in trying to explain the atmospheric dynamics and surface characteristics. © 2002 Elsevier Science (USA)

Key Words: Titan; Titan's aerosols; tholins; complex refractive index.

1. INTRODUCTION

Solar photons with wavelengths between 100 and 160 nm photolyze methane and its principal products, the C₂ hydrocarbons, in the upper atmosphere of Titan. Energetic electrons coming from Saturn's magnetosphere dissociate molecular nitrogen, the dominant background constituent, leading to reactive N atoms. The primary products of these chemical interactions evolve to heavier organic compounds composed by C, H, and N that are likely to associate to form the particles of the haze layers that hide Titan's surface. Three haze layers have been recognized: two of them located between the 0.1 and 0.01 mbar pressure and the detached one visible in the ultraviolet, located above the 0.002 mbar pressure (Atreya 1986, Morrison *et al.* 1986). The variation in brightness in Titan's disk was the first source utilized to get information on the nature, distribution, and properties of aerosols as summarized in Hunten *et al.* (1984). This

information has been complemented with experimental work. Laboratory simulations of Titan's atmosphere environment have demonstrated that long-time irradiations of CH_4 and N_2 mixtures with different energetic sources yields sticky, dark-color condensed materials proposed as good candidates to characterize Titan's aerosols (Sagan and Thompson 1984, Khare *et al.* 1984, Scattergood *et al.* 1989, Thompson *et al.* 1991). However, important differences in their properties have been found because they strongly depend on the experimental conditions used to obtain the tholin materials, such as initial gas mixing ratios, irradiation time, and energy source, leading to differences in parameters such as the size, shape, chemical composition, and optical properties. The correct characterization of the properties, especially the optical ones, of an analogue that well resembles Titan's stratospheric aerosols is highly essential owing to the important role that the aerosols have in the radiative transfer processes in the atmosphere, which are responsible for, among other things, the atmospheric temperature profile (McKay *et al.* 1989, McKay *et al.* 1991, Samuelson and Mayo 1991) and surface temperature value (Danielson *et al.* 1973, Samuelson, 1983). The interpretation of a variety of atmospheric remote-sensing data also requires knowledge of the optical properties of the aerosols, which can be described in terms of the complex refractive index, to compute good reference models (McKay *et al.* 1989, Griffith *et al.* 1991, Coust enis *et al.* 1995). Direct characterization of Titan's aerosols is currently impossible; therefore, the experimental approach becomes the best way to understand the physical and chemical properties of the aerosols and to make progress in the interpretation of their role in Titan's upper atmosphere.

Khare *et al.* (1984) performed the first study under well-controlled experimental conditions and specially designed for the characterization of the complex refractive index of an analogue of Titan's aerosols. These authors determined the real (n) and imaginary (k) parts of the complex refractive index of the resulting product from a 15-mA direct current (DC) electrical discharge through a 0.2 mbar $\text{N}_2 : \text{CH}_4$ (9 : 1) gas mixture maintained by a 200-V potential difference between the electrodes and constantly flowing through a 1-l chamber at a rate of approximately $0.05 \text{ cm}^3 \text{ s}^{-1}$. This material was referred to as "Titan's tholin" (Sagan and Thompson 1984) and was believed to adequately reproduce the aerosols expected for Titan's atmosphere. Khare and co-workers performed independent transmittance, reflectance, interference, and polarization measurements of Titan's tholin films deposited on glass or alkali halide substrates to obtain n and k from the soft X-ray to the microwave region. Due to the wide wavelength range studied, they made some sets of measurements within different spectral ranges and then used a Kramers–Kronig treatment to adjust the experimentally determined values to the calculated ones to get the entire n and k spectrum. These results have been used during the past seventeen years by several investigators and have formed the basis for a long series of interpretations (see, for example, the works of Rages and Pollack (1980) for the geometric albedo, Griffith

et al. (1991) for the surface and tropospheric characteristics, and Lorenz *et al.* (1999) for the HST images) and microphysical models (for instance, the ones presented by McKay *et al.* (1989), Toon *et al.* (1992), and Rannou *et al.* (1995)). The experimental work performed by Khare *et al.* (1984) in calculating the complex refractive index of Titan's tholins was scrupulously organized. Their values, correct within the experimental error of $\pm 3\%$ in the measured n values and $\pm 30\%$ in the measured k values, have been useful for the majority of the modeling works. Nevertheless, the use of a correction factor that varies with wavelength is always necessary to accomplish a good fit of the data. In the frame of the program to study the characteristics of Titan's aerosol analogues, Coll *et al.* (1999) characterized, by their infrared spectrum, the solid phase synthesized during simulation experiments performed under the most realistic possible laboratory conditions. When comparing their tholin spectrum to that of the tholins synthesized at Cornell University and used by Khare *et al.* (1984) for the calculation of the complex refractive index, several qualitative differences were encountered. This unexpected outcome led us to initiate a detailed study of the optical characteristics of this material. We present here a new set of values for the real and imaginary parts of the complex refractive index, defined by $m = n + ik$, of a laboratory analogue of Titan's aerosols. Improvements in the aerosol analogue quality have been made. We recovered the aerosol films directly deposited on quartz plates, under an inert atmosphere. Our n and k values are directly calculated from the transmittance and reflectance values exhibited by our samples in the 200–900 nm range and include 160 experimental points. The influence of sample thickness uncertainty, aerosol porosity, and amount of scattered light on the final n and k is calculated and discussed. Instead of presenting absolute values for the complex refractive index parameters, we have determined an interval within which they can be located. Our data can be seen as a new point of reference to modelers who compute the properties of Titan's aerosols and can be used to see how their optical properties influence the matching of the observed atmospheric spectra. This article is organized as follows: Section 2 describes the synthesis of the aerosol analogues. Section 3 briefly describes the optical methods utilized and the calculations performed for the calculation of n and k . The results are presented and discussed in Sections 4 and 5. Section 6 summarizes our conclusions.

2. AEROSOL ANALOGUE SYNTHESIS

An $\text{N}_2 : \text{CH}_4$ (98 : 2) gas mixture was subjected to a DC cold plasma discharge, resulting in the production of thin films of yellow to light brown solid reaction products. We selected the methane content in our mixture from its mole fraction value estimated for Titan's stratosphere after the reanalysis of Voyager 1 measurements by different techniques (Lellouch *et al.* 1989, Kouvaris and Flasar 1991, Strobel *et al.* 1993, Courtin *et al.* 1995). The simulated atmosphere has therefore a closer similarity to Titan's stratospheric conditions than does the crude mixing

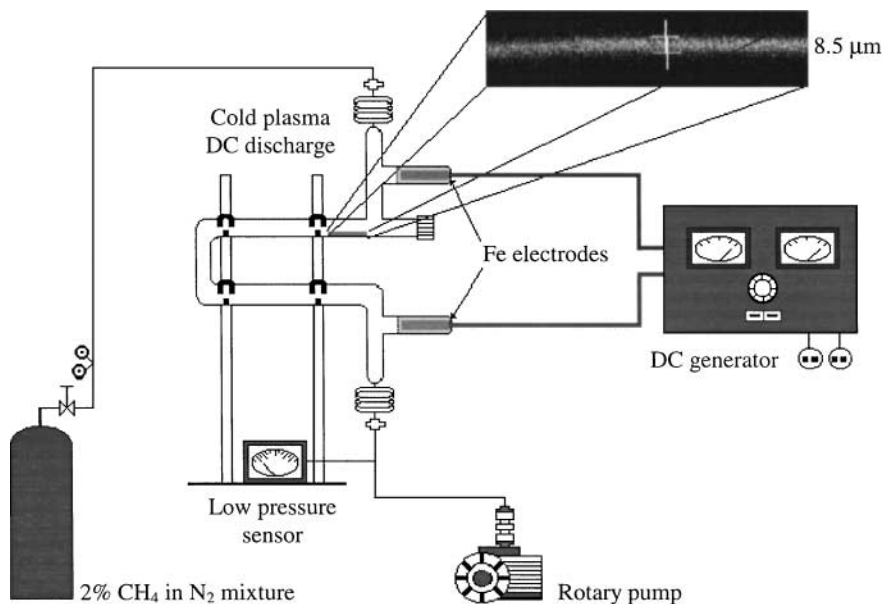


FIG. 1. Schematic representation of the experimental continuous-flow setup used to produce Titan's aerosol analogues after irradiation of a $N_2 : CH_4$ (98 : 2) mixture by a glow discharge. Inset: Z plane of a Titan aerosol analogue film, as observed under the confocal microscope showing the granular morphology of the deposit.

ratio of 10% methane used in the simulation experiments performed during the 1980s. The implications of this selection are discussed in Section 5.

The experimental setup is shown in Fig. 1. The mixture (99.9995% purity from Linde) continuously flowed to a Pyrex reactor in which the cold plasma discharge took place. The reactor vessel was 25-cm long with 18- and 9-mm internal diameter upper and lower arms, respectively, and extensions of 18-mm internal diameter with condensing spirals for the input and output of the reactant gas mixture. A rotary pump was used to allow the transit of the gas mixture. The pressure, 1 mbar at room temperature, was controlled with a needle valve attached at the exit of the reactant mixture tank and its value was read in a low-pressure sensor. A stainless steel flexible hose and stopcocks were used to fasten the reactor to the mixture's tank and to the rotary pump. The DC cold plasma discharge was generated by a potential difference of ~ 4 kV between two iron electrodes, covered with mica to avoid metal contamination. Iron was selected for its good physical and electrical properties, its high melting point, and low ionization potential. The electric potential difference is established by a high-impedance DC generator with maximum current output of 200 mA. The reactor was topped with a plastic cap that permitted placement of adequate optical quality substrates on the upper arm for the solid-product deposition and later analysis. Films of the solid products were also observed on the reactor arm walls.

Thin films of our aerosol analogues produced with different irradiation times with the cold plasma discharge maintained at 280 W were deposited on quartz slides (12×45 mm, Suprasil). For a sample exposed during 1-h irradiation time, a pale orange-

brown transparent homogeneous film could be seen by the naked eye. Stronger coloration intensities could be observed when the irradiation time was increased. Due to the spectroscopic technique selected to perform the study, we can only work with transparent samples. After analyzing the transmittance curves obtained for 1-, 2-, 4-, 8-, and 10-h, irradiation, we decided to perform the calculations of n and k only on the samples produced after 120 and 240 minutes of irradiation (samples 2H and 4H respectively) because they exhibited the best transparency. The region of the plasma discharge remained in close contact with the slide surface during the entire irradiation time. It was observed that in the course of an experiment the current input had to be increased to maintain a constant power value. This can be attributed to an increase in the total resistivity of the system (i.e., the gas-phase reactant mixture and the formed solid film). Increments of some 2 to 4 mA were necessary to keep a constant value of 280 W during the entire irradiation time. Although a formal estimation of this variation was not performed, for the 2H sample the final current value was around 82 mA, while for the 4H sample it was around 92 mA.

The protocol developed at LISA allows sample recovery without terrestrial atmospheric contamination. An elemental composition analysis was performed on one of our samples, produced as described above, in the Microanalysis Service of CNRS, Gif-sur-Ivette, France. The amounts of carbon, nitrogen, and hydrogen, were determined by combustion and that of oxygen was determined by calculation (completion to 100%). Samples are prevented, as much as possible, from any contact with potential atmospheric contaminants (O_2 , CO_2 , H_2O vapor). Once the irradiation was stopped, the samples were kept in polystyrene

bags, under an inert atmosphere of nitrogen, and these remained closed until the spectroscopic measurements were done. One oxygen atom for every 150 atoms of C, H, and N was found. These results seem very low compared with those reported by previous experimental syntheses of Titan's aerosols. Sagan *et al.* (1984) reported an oxygen content of 17% in the Titan's laboratory tholin. McKay and Toon (1992) suggested that the presence of oxygen was the result of oxidative processes occurring when the tholin was allowed to have contact with the atmosphere. McKay (1996), using an experimental setup similar to that of Sagan *et al.* (1984), produced a brown material that still had a high oxygen content. He reported values of up to 12% oxygen atoms, which means the presence of 1 oxygen atom for every 15 C, H, and N atoms. The implications of these differences are discussed in Section 5.

3. OPTICAL MEASUREMENTS AND CALCULATIONS

The heterogeneity of our samples, their roughness, and their nonuniform thickness limited the choice of the optical techniques and methods usable to correctly determine the complex index value. We therefore chose reflectance and transmittance measurements and solved the Abelès equations (Abelès 1967) for thin films provided the film thickness is known.

3.1. Film Thickness Measurements

The fluorescence of the aerosol analogue films was excited with a wavelength of 488 nm (argon laser) and the films were observed with a confocal microscope (Zeiss LSM 410) to determine their thickness. A lens with a 63 \times magnification and a 1.4 aperture was used. The pinhole was set to give resolutions of 0.21 μm in the *XY* plan and 0.52 μm in the *Z* direction. The inset shown in Fig. 1 represents a *Z* section of an aerosol film. Film thicknesses of $3 \pm 1 \mu\text{m}$ for the 2H irradiation sample and $4 \pm 1 \mu\text{m}$ for the 4H irradiation sample were deduced from the *Z* confocal images. Even if limited in its intrinsic accuracy, this method gives a good estimate of the mean thickness because its variations along the film are directly visualized. Moreover, these confocal images point out the porosity of the aerosol analogue films, allowing a rough estimate of its value at less than 0.3 to be made in these samples.

3.2. Transmittance and Reflectance Measurements (Specular and Diffuse)

Specular transmittance and reflectance measurements were performed on samples 2H and 4H from the near ultraviolet (200 nm) to the near infrared (900 nm) by using a Cary 5 (Varian) spectrophotometer. The corresponding 4-h irradiation sample plots are shown in Fig. 2. Typically, the specular optical properties are observed on mirrorlike surfaces. This does not mean, however, that the aerosol analogue films behave like mirrors. They are transparent enough to allow the transit of the incident radiation through the quartz plate, behind which a standard mirror is placed. In this way, the one-to-one correspondence

between incident and reflected or transmitted rays can be obtained. During the reflectance measurements the incident ray, the corresponding reflected rays, and the normal to the surface at the point of incidence all lie in the same plane. This is the traditional way of measuring the reflectance of a surface or medium. In our samples, transmittance measurements were made under normal incidence while reflectance measurements, performed with a V-W attachment, were made under an 8° incidence. To check the reproducibility of our deposition technique, we measured the specular transmittance of two different 4H samples prepared under the same deposition conditions, but at different times. Figure 2a points out the excellent similarity displayed by the two samples and achieved by our experimental technique. This similarity is a remarkable achievement of the present work, since previous experimental simulations have not obtained good reproducibilities of the transmittance measurements, even when performed on the same sample. Such is the case of the set of transmittance graphs determined by McKay (1996) from samples of different methane mixing ratios (see Fig. 6).

We also performed transmittance and reflectance hemispherical measurements on sample 4H with an integrating sphere to measure the light scattered by the sample, which is not taken into account in the specular measurements. The term hemispherical is applied to the fraction of a given incident flux that is usually reflected to all directions from a mirror like surface or medium. This fraction of flux corresponding to a given wavelength range is captured by a special device known as an integrating sphere. In this way, it is possible to complement the one-to-one measurements performed in the specular mode. The amount of scattered light is less than 0.05 in transmittance and less than 0.015 in reflectance, corresponding to scattering ratios respectively of the order of 5.5% and 19%. The scattering is therefore not negligible and must be taken into account in the complex refractive index calculations.

The curves in Fig. 2, especially the reflectance ones, show oscillations due to interference in the thin films. Theoretically, the product $n \times d$ (refractive index multiplied by thickness of the film) might be deduced from these interference patterns (Swanepoel 1984). However, one can notice that the transmittance and reflectance interfringe peaks and valleys do not match. This is due to the nonuniform thickness of our low-quality optical samples (which nevertheless do not destroy the interference phenomenon) coupled with the fact that the area sampled by the measurement beam is slightly different in transmittance and reflectance. The presence of inhomogeneities drastically changes the spectra, and the formulas used for uniform films are no longer valid (Swanepoel 1984). We therefore got only an estimate of the product $n \times d$ by using this interference pattern. To make our measurements independent of these incompatible interference patterns in the optical spectra for the calculation of the complex index, we treated these measurements to suppress the effect of coherence (Grigorovici *et al.* 1982, Swanepoel 1984, Demichelis *et al.* 1987). The result of this treatment is shown on the 4H reflectance curve in Fig. 2b.

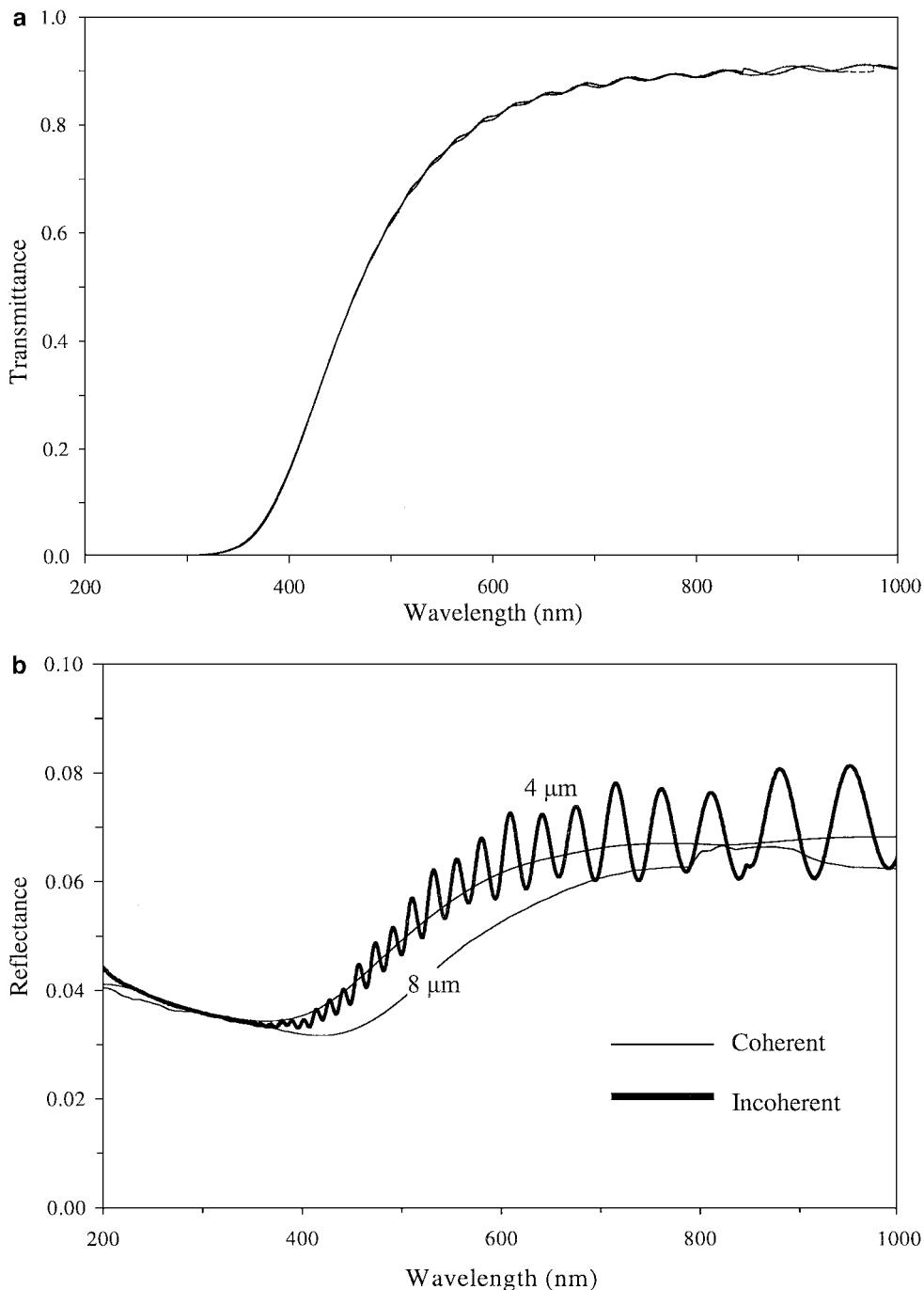


FIG. 2. Transmittance (a) and Reflectance (b) values as a function of wavelength of Titan's aerosol analogues produced from a 2% CH₄ in N₂ gas mixture after a 4-h irradiation with a DC cold plasma discharge. The thickness of the aerosol analogue layer is $4 \pm 1 \mu\text{m}$. Figure 2a shows the transmittance curves of two different 4-h samples. They exemplify the reproducibility and high accuracy of our experimental techniques. Figure 2b shows the oscillations in the reflectance values due to the interferences that the aerosol analogue films induce in the light pathway. The reflectance graph obtained after suppressing this coherent effect is also shown. The lowest curve in Fig. 2b represents the reflectance data of an 8- μm sample.

3.3. Complex Refractive Index Calculations

In addition to the wavelength the reflectance (R) and the transmittance (T) values depend on the following parameters:

1. refractive index, n ,

2. extinction coefficient, k , and
3. mean thickness of the film, d .

Following the Abelès formulas established for the case of incoherent thin films (see Appendix) n and k values are extracted

wavelength by wavelength in the range 200–900 nm, from the 160 experimental points using a weighted gradient method. This is clearly a difference from the multiple methods used by Khare *et al.* (1984) (Kramers–Kronig, ellipsometry, interference, Brewster angle), which allowed these authors to get a continuous determination of k from 10 measurements in the 200–900 nm spectral range.

4. RESULTS AND DISCUSSION

4.1. Transmittance and Reflectance

Qualitatively, it can be seen (Fig. 2) that our films absorb light below 500 nm and their transparency increases beyond this wavelength. Therefore, they display a behavior similar to that observed in Titan's aerosols (Rages and Pollack 1980, Neff *et al.* 1984): They are highly absorbing in the ultraviolet. A deposition rate, under our experimental conditions, of approximately 1 μm film thickness per irradiation hour was also estimated.

If a comparison between our resulting transmittance curves and those reported by previous experiments is done, there are some particularities about the aerosol films that we must recall. It has been suggested that the optical properties are highly dependent on a number of experimental consideration such as the $\text{N}_2 : \text{CH}_4$ initial gas mixture ratio, the selection of energy source and its intensity, the pressure and temperature of the reactant mixture, and the contamination of the samples by the laboratory atmosphere (Coll *et al.* 1999). It seems that the differences in the conditions under which aerosol analogues are produced is a barrier to the complete understanding of the solid organic phase produced in the laboratory. Despite this problem, the transmission curves of thin films of tholin produced by irradiation with a Tesla coil (McKay 1996) and by a radio-frequency discharge (Khare *et al.* 1987) in $\text{N}_2 : \text{CH}_4$ mixtures with different ratios and thickness have been compared by McKay (1996). The procedure used in that paper for comparing the transmittance curves of samples with different thickness and compositions consisted in normalizing the transmittance of the different samples to the fixed value of 0.9 at a reference wavelength of 750 nm. This comparison is meaningless for the transmittance and reflectance, which depend on the thickness of the films (see Appendix). The thickness value is unknown in McKay's samples and is considerably variable in Khare's samples. A correct comparative discussion of the intrinsic optical properties of these samples can only be made on their complex index or dielectric function. Nevertheless, a comparison is possible on the transmittance (or the reflectance) curves if the samples to be compared have the same thickness, or, at least if their thickness is known. In the latter case, a comparison of the extinction coefficients (k) can be made, through a crude evaluation of its values from the transmittance by using the approximation $T = T_0^2 \exp(-\alpha d)$ with $\alpha = (4\pi k)/\lambda$ and T_0 being the transmittance at the interfaces, assumed to be the same for the different films and independent of the wavelength (Abelès 1967). Because the thicknesses of the films compared by McKay (1996) in his paper were not

determined, it is impossible to apply this approximation to the treatment of their transmittance values. We will therefore only compare, at the end of this paper, our results on the complex index with similar results available in the literature.

4.2. Complex Refractive Index

We present n and k spectral variations of two samples (2H and 4H) in Fig. 3. They qualitatively look like quantities related by causality (Kramers–Kronig relations), which means that n presents an inflection point at a wavelength where k exhibits a maximum. This happens while n decreases from low to high wavelengths. From Fig. 3b, the maximum k value (0.051) is located at 315 nm for sample 2H; for sample 4H it is located at 290 nm and has a value of 0.044. The inflection points in the n graphs, even when they are not very evident in Fig. 3a, must be located around the wavelengths of these k maximum values. The two samples are supposed to differ only in their thickness. They should therefore exhibit the same n and k values within the experimentally determined thickness uncertainty. It is well verified on n , where the values show errors of $0.022 \pm 0.04\%$ for the 2H sample and $0.026 \pm 0.04\%$ in the case of the 4H sample. However, k spectral values differ more perceptibly. The calculated error value for the 2H sample is $35.24 \pm 0.12\%$, while for the 4H sample it is $25.98 \pm 3.23\%$. These discrepancies can be attributed either to different chemical compositions or to different morphologies of the samples. They can also, more simply, be due to the effect of the uncertainties in the knowledge of some parameters or effects that act on the measured optical properties. The observed similarity in the transmittance values of samples 2H and 4H (Fig. 2a) obtained from different deposited films eliminates the validity of differences in the composition of our samples. On the other hand, the roughness and nonuniformity in thickness displayed by our aerosol analogues, parameters directly related to the morphology, made us consider the influence of thickness uncertainties, porosity, and light scattering to explain the discrepancies on the value of the complex index.

4.3. Influence of Sample Thickness Uncertainty

Due to the relatively large uncertainty in the thickness measured from our samples, we have made the calculation of n and k for the mean and extreme values of d to get boundaries for their variation (Figs. 3a and 3b). On sample 2H, $d = 3 \pm 1 \mu\text{m}$. On sample 4H, $d = 4 \pm 1 \mu\text{m}$. The n values are not strongly affected within the range of variation (Fig. 3a). In contrast, k strongly decreases as thickness increases (Fig. 3b). These results follow the qualitative dependence of R and T on n , k , and d in the framework of the incoherent optical treatment that we applied to our samples. On the one hand, $R = [(n - 1)^2 + k^2]/[(n + 1)^2 + k^2]$ essentially depends on n for small k values. As k values are two orders of magnitude smaller than the n values, the equation for R can be rewritten as $R = [(n - 1)^2]/[(n + 1)^2]$. On the other hand, $T = T_0^2 \exp(-\alpha d)$, with $\alpha = (4\pi k)/\lambda$, depends on the

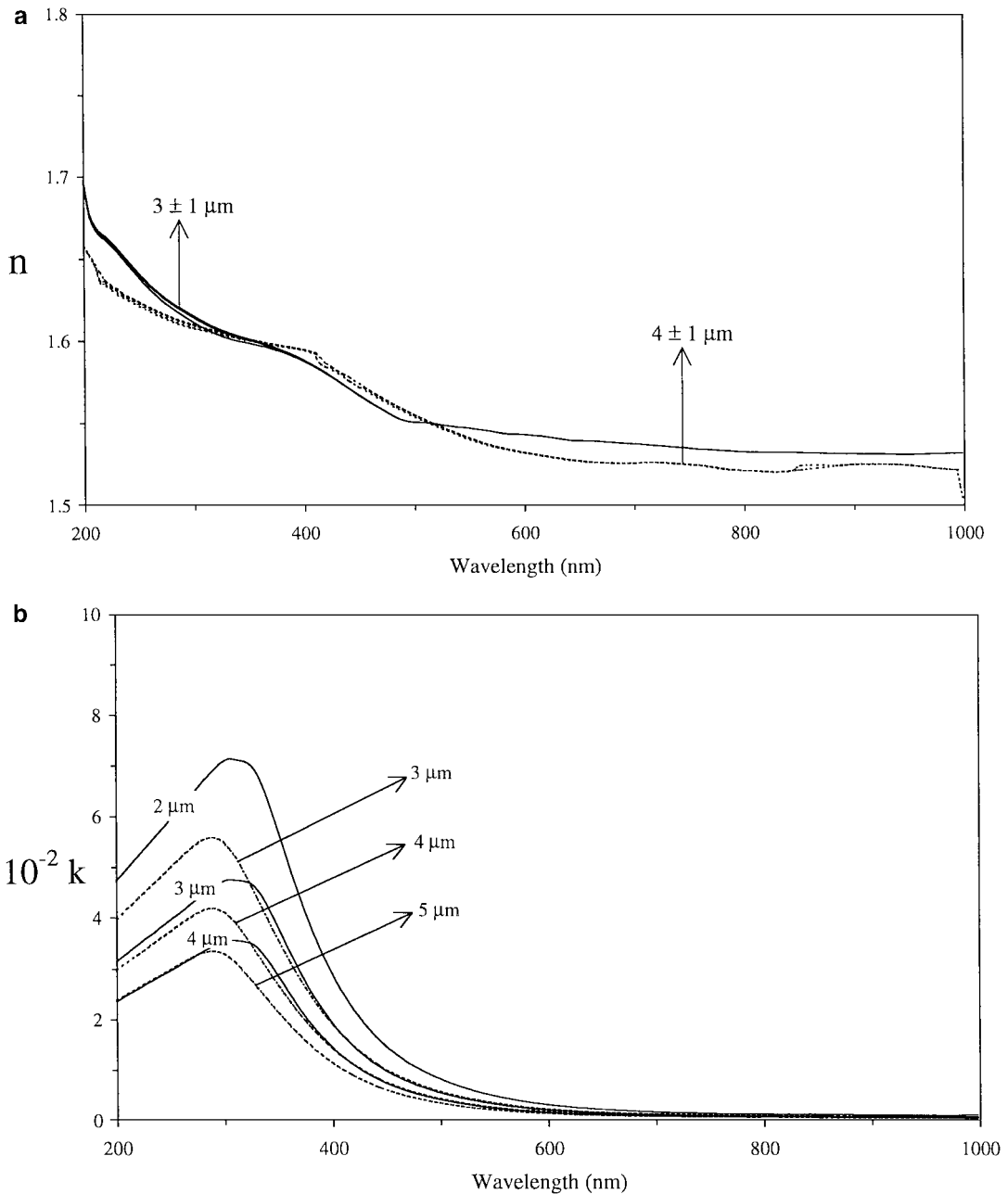


FIG. 3. Influence of the film thickness uncertainty on the evolution of n (a) and k (b) as a function of wavelength. Solid curves correspond to a 2-h irradiation sample; dashed curves are from a 4-h irradiation sample.

product $k \times d$. Therefore, for a given experimental value of T , a variation of d will essentially affect the k values to keep the product $k \times d$ constant. The behavior of n is very similar for the two samples; in both cases it monotonically decreases from 1.68 to 1.53 between 200 and 900 nm. The behavior of k shows a displacement in the maximum value occurring, respectively, at 325 nm and 300 nm for 2H and 4H samples. Nevertheless, the position of this maximum is not affected by the variations of the thickness. Other parameters not directly involved in the for-

mula of n and k , for example, the porosity and roughness of the samples, may influence their values and their spectral variations.

4.4. Influence of Porosity

Coll *et al.* (1998) had previously pointed out the porous nature of the aerosol analogues using scanning electron microscopy. The same was observed by de Vanssay *et al.* (1999) who studied the variation of tholins morphology under different experimental

TABLE I

Maximum Values of Refractive Index (n) and Extinction Coefficient (k) for Titan's Aerosol Analogues as a Function of Porosity (p)

Air content, p	0.0	0.1	0.3	0.5
Refractive index, n	1.000	1.038	1.144	1.370
Extinction coefficient, k	1.000	1.111	1.408	2.163

Note. Values are normalized to 1 for $p = 0$. The figures represent the multiplicative factor that must be applied.

conditions. These authors find that the CH_4/N_2 ratio has a strong effect on the tholin morphology. Neither differences in the total pressure nor in total flux affected particle size. Nothing is concluded about the porosity values of the samples. However, some of the pictures included in their paper show the porous nature of the tholins. Those observations have been confirmed using the present experimental simulation by observing different samples under confocal microscopy (see the inset in Fig. 1, for example). We thus have deduced very approximate values of the porosity in the 2H and 4H aerosol analogue samples from their micrographs. We evaluated the variations of n and k for a range of air content between 0 and 50%. We used the effective medium model of Maxwell-Garnett (Maxwell-Garnett 1904) for this calculation. The effect is essentially a uniform increase of n and k with increasing porosity values and a very slight shift of the k maximum toward short wavelengths. We therefore approximate this uniform increase by a multiplicative factor. Its maximum values, for the two samples in the porosity range from 0.0 to 0.5, are represented in Table I. One can observe that the air content has a strong influence on n and k . For example, increasing the porosity in the sample to 0.3 induces an increase of 41% in k and of 14% in n .

4.5. Influence of Light Scattering

The calculations of the complex refractive index values presented above were performed using the specular measurements. We have shown in Section 3.2 that the amount of scattered light measured on our samples is not negligible and must be considered in the calculation of the complex index parameters. The calculations performed with specular measurements take into account reflectance and transmittance measurements lower than the total values measured when using an integrating sphere. This leads to an underestimation, mainly of the absorption coefficient k . Figure 4 shows the n and k values computed from the specular and hemispherical measurements of transmittance and reflectance performed to sample 4H. A qualitative comparison between the two sets of values can be made. As observed from Fig. 4a, the n values are not so strongly affected. They exhibit a relative uniform increase of about 5% through the entire wavelength range. Figure 4b shows two important things: (i) that the maximum k value increases at approximately twice its specular value and (ii) that its position has been shifted from 350 to 300 nm. The decreasing effect vanishes toward long wavelengths.

5. DISCUSSION

To summarize the effects of the different parameters envisaged above we have plotted mean values of n and k in Fig. 5. The graphs are the result of 160 transmittance and reflectance experimental measurements. The error bars resulted from the effect of the sample thickness uncertainty and of the scattered light on the n and k calculated values. In the same graphs, we show the results of Khare *et al.* (1984). In this section we present some arguments to explain the observable differences. One must first recall that the two plotted sets of values were calculated from different protocols and from samples synthesized under different experimental conditions. As mentioned in Section 4.1, previous experiments (McKay 1996) have demonstrated a strong variation of the transmittance values on thin films of tholin material produced from mixtures with different CH_4 concentrations, as illustrated in Fig. 6. There is also a disagreement in the transmittance values between the tholins produced with the same initial CH_4 mixing ratio but using different techniques, as demonstrated in the same paper by McKay when he compares his work with that of Khare *et al.* (1984). We have no evidence to state that the differences between our calculated complex refractive index values and those existing in the literature are due only to the difference in composition. No reported study exists where a wide systematic variation of methane content and calculation of the complex refractive index have been performed following the same experimental and mathematical procedure. We present here the first attempt to initiate such a study. We imply that there must be a relationship between the initial methane content and the final optical properties of Titan's aerosol analogues, but we would need to produce an exhaustive experimental and mathematical work before arriving at a confirmation. Before proceeding to a direct comparison of our results and the values of Khare *et al.* (1984) we must take into account that the porosity will apply a multiplicative factor larger than 1 to these values (see Table I), especially to the extinction coefficient values that remain one order of magnitude lower with respect to those of Khare *et al.* (1984). This correction does not modify, however, the shape of the curves. Consequently, our results look considerably different from those of Khare and co-workers. The variations in our n values are much less contrasted and weaker. The resulting graph lacks the structure between 100 and 400 nm observed in Khare's *et al.* (1984) graph. A maximum in k in the near UV (300 nm) is observed in our values but is not present in Khare's *et al.* (1984) results. These characteristics indicate that our values follow more closely the causal relationship between n and k curves even when they were not calculated using the Kramers–Kronig technique.

We have pointed out the main differences that exist between our work and previous determinations of optical properties of Titan's aerosol analogues. We now attempt to explain the way by which the intrinsic parameters of our aerosol analogues can contribute to these differences. The difference in the methane content is considered first. One of our main objectives was to perform the synthesis of the aerosol analogues in an environment

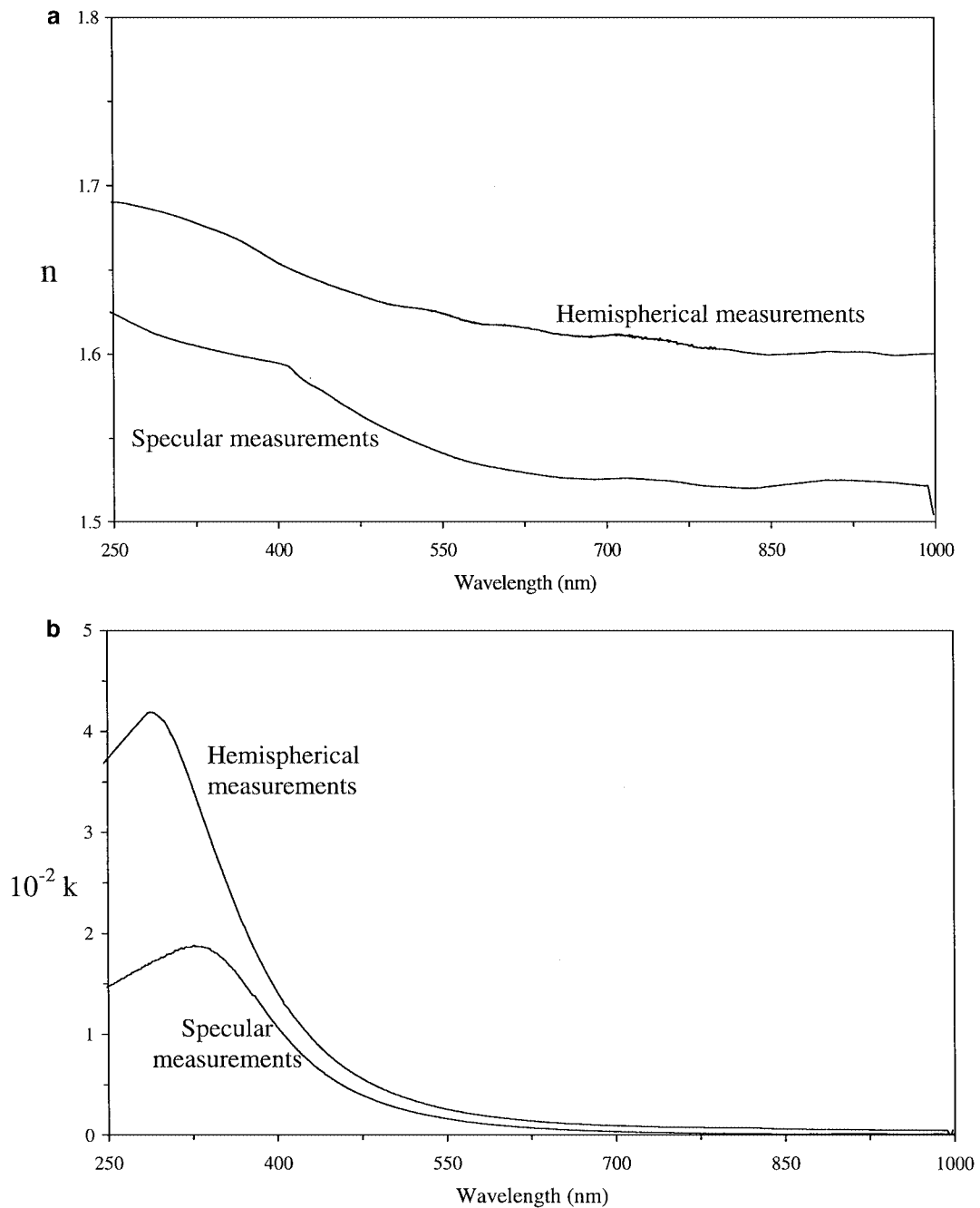


FIG. 4. Evolution of n (a) and k (b) as a function of wavelength for a 4-h irradiation sample. The two sets of graphs resulted from transmittance and reflectance measurements performed in the specular and hemispherical modes.

that resembles that of Titan's stratosphere. Besides temperature, the other more significant parameter in the synthesis of the aerosol analogues is the initial methane content. We have selected the methane mixing ratio of our simulated stratosphere based on existing information. Several different reanalyses of the Voyager data can exemplify this: Lellouch *et al.* (1989) determined a wide methane mole fraction range (0.5 to 3.4%) for the stratosphere of Titan from the refractivity profiles of the radio-

occultation experiment. Kouvaris and Flasar (1991) delimited the values to a CH_4 mole fraction of $1.7 \pm 0.1\%$ from the cold trap up to the stratosphere. Strobel *et al.* (1993) determined a stratospheric methane mole fraction $\leq 2.6\%$ from a reanalysis of the Voyager UVS solar-occultation measurements. The most recent determination is the one done by Courtin *et al.* (1995), who, upon reanalyzing the Voyager infrared measurements, expanded the range of the CH_4 mixing ratio from 1.7 to 4.5%

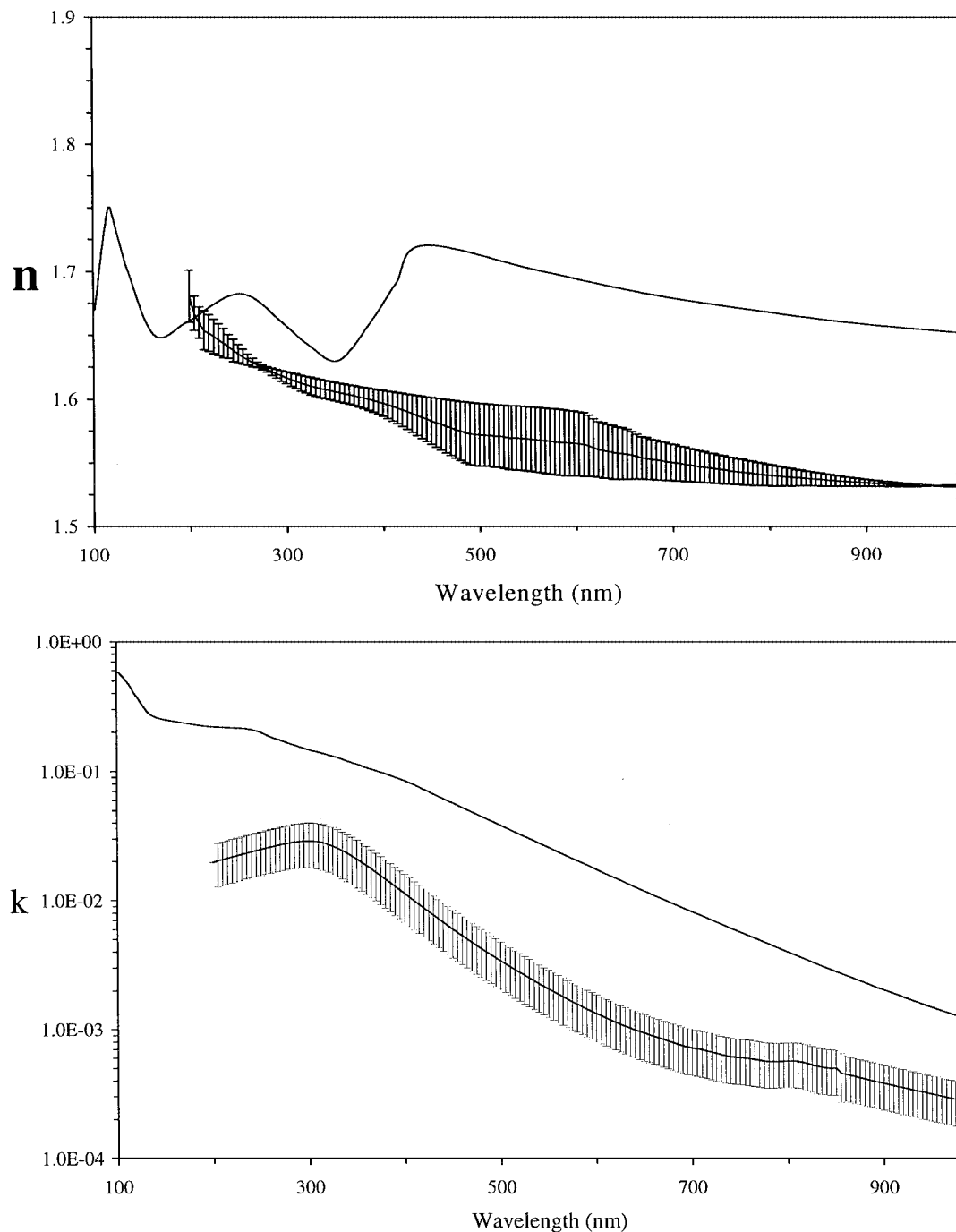


FIG. 5. Final values for the n and k parameters determined from our Titan aerosol analogues including the thickness and scattering effects. Khare *et al.* (1984) values correspond to the curves without error bars.

in the stratosphere. Thus we selected the value of 2% methane content as the most representative for Titan's upper atmosphere, according to the actual estimations.

Scattergood *et al.* (1988) were the first to suggest that the optical properties of Titan's tholin depend on the CH_4 to N_2 ratio in the initial gas mixture. Some years later, McKay (1996), using an experimental setup similar to that of the Cornell group, pre-

pared thin films of the "Titan tholin." The films were deposited on quartz slides and were prepared with CH_4 mixing ratios varying from 3 to 100%. A plot of transmission versus wavelength shows reproducible curves when the measurements were performed on different locations in the same sample, as illustrated in Fig. 6 by the different curves of 20 and 70% CH_4 content. However, variations of more than a factor of 2 were found on

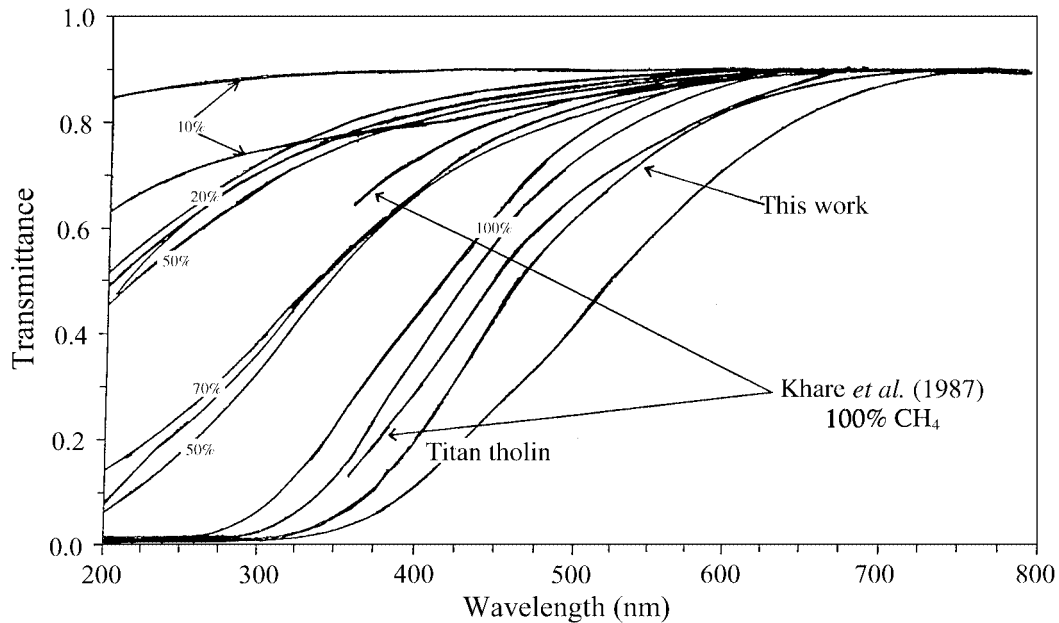


FIG. 6. Transmittance curves as a function of wavelength of the solid material produced from mixtures with different methane mole fraction. Modified from McKay (1996). The curve labeled as "This work" has thickness of $4 \pm 1 \mu\text{m}$.

samples that had the same initial amount of methane but had been deposited on different slides. This is the case of the 10, 50, and 100% CH_4 curves presented in the same figure. McKay (1996) compared his results with those of Khare *et al.* (1984) and found that the Cornell's tholins were darker for similar experimental conditions (see Fig. 6). From these results McKay confirms that the optical properties of laboratory tholins strongly depend on the CH_4 to N_2 ratio. He found a darkening in the tholin material with increasing methane concentration. However, he did not find an explanation for the disagreement between the optical properties of his tholin and that produced by Khare *et al.* (1984). Our transmittance results for a 2% methane content are within the range of values reported by Khare *et al.* (1984) and McKay (1996), as shown in Fig. 6. All sets of data have a similar wavelength dependence. This is important because the observed slope has been considered as a fingerprint for Titan's aerosols. However, it is not possible to perform a direct comparison of the results, as explained in Section 4.1, owing to the lack of thickness measurements in the case of McKay's study. In contrast, a wide range of thicknesses, from 0.6 to $20 \mu\text{m}$, is reported for the samples of Khare *et al.* (1984). This causes a problem when trying to compare the magnitude of the absorption using the Abelès formulas, since Khare *et al.*'s (1984) samples do not exhibit single values but an extended interval within which we can place the absorption of our 2H and 4H samples.

Another parameter that can contribute to explaining the observed differences is the absence of contamination. From the elemental composition analysis we can affirm that our samples do not significantly incorporate terrestrial atmospheric gases (O_2 , CO_2 , H_2O vapor). As explained in Section 2 this kind of contamination was not determined in Khare *et al.*'s (1984) work.

We cannot establish any correlation between the shapes of our n and k graphs and the absence of contamination. We infer that they can, in part, be explained by this fact, which at the same time strengthens the quality of our aerosol analogues. Another difference that must be mentioned is the time the samples were exposed to the discharge irradiation. The "Titan tholin" (Khare *et al.* 1984) was irradiated by three days and resulted in samples of 0.6- to $20\text{-}\mu\text{m}$ thickness. McKay (1996) irradiated his samples for three weeks but did not determine the thickness of his samples. We performed the irradiation during 2 to 4 h and got samples 2- to $5\text{-}\mu\text{m}$ thick. It is evident that the main effect of over-irradiation is the growth of the sample. This has, as a consequence, a darkening that is evident from the transmittance graphs (see Fig. 6). The reflectance data for the $8\text{-}\mu\text{m}$ sample have been added to Fig. 2b. They represent an upper limit of the reflectivity that may exhibit a layer of a solid material, similar to the aerosol analogues that we have synthesized in the present work, deposited on the surface of Titan.

The chemical transformation of the simulated stratosphere was performed by a glow discharge. The main propagation mechanism for this type of discharge is the electron impact. In addition, it emits a considerable fraction of radiation that corresponds to wavelengths in the visible and ultraviolet domain (Chang *et al.* 1991). The cold plasma generated by the glow discharge is very active and energetic and allows the dissociation of the initial CH_4 and N_2 molecules. At the same time it avoids the existence of the very high temperature gas environment typical of the hot plasmas produced by electrical discharges generated by Tesla coils or by laser beams. The main driving mechanism in Titan's upper atmosphere is UV radiation; this means an energetic source that produces cold

plasmas. By using a glow discharge we are ensuring that we are not initiating a chemistry different from that produced by energetic saturnian electrons and short-wavelength UV solar radiation.

6. CONCLUSIONS AND APPLICATIONS TO TITAN

We synthesized Titan's aerosol analogue films free of laboratory contamination using an initial gas-phase mixture that closely resembles the satellite's stratosphere. The heterogeneity and roughness recognized in our samples guided our selection in the optical techniques used to more accurately estimate their complex optical index. We discussed and graphically represented the influence of film thickness uncertainty, amount of scattered light, and porosity in the n and k values, with the extinction coefficient (k) being the most affected. As observed in Figs. 3 and 4, an increase in the film thickness and a smaller amount of recovered scattered light resulted in a decrease in the maximum k value. As the k curves decrease toward long wavelengths the effect weakens. Table I shows that the porosity affects k in a reverse way and considerably higher values are calculated for high porosity levels. We summarize the effect of the studied parameters in Fig. 5 and tabulate the n and k values with their uncertainties in Table II. The data are available on the Internet at http://www.astroquimica.nuclecu.unam.mx/Titan_nk.html. Within the wavelength domain of 200–900 nm n varies from 1.53 to 1.68 and k varies from 2.62×10^{-4} to 2.87×10^{-2} . It is important to notice that, regardless of the differences in magnitude, our work shows a k slope similar to that displayed by the "Titan tholin" synthesized by Khare *et al.* (1984). This slope has been considered as a fingerprint for the stratospheric aerosols of Titan. Sagan and Thompson (1984) demonstrated that no other material, different from the solid produced by irradiation of methane and nitrogen mixtures, exhibits the reflectivity necessary to match the observed reflectivity of Titan at wavelengths uncontaminated by methane absorption bands. The slope observed in the solid produced by laboratory simulations is consistent with available observations of Titan in the infrared and ultraviolet. The visionary nature of the work of Khare and Sagan performed seventeen years ago remains. They anticipated astrobiology and used the best cutting-edge techniques in pioneering research available at their time to obtain useful results. We have demonstrated, however, that improvements in the synthesis methodology, simulation machinery, and calculation methods yield different but also valid results. Information about Titan's atmosphere and surface is constantly being derived from direct or ground-based observations. To satisfactorily explain these observations, models need to be computed with information that comes, in most of the cases, from experimental simulations. The results that we present here need to be tested against the latest Titan's geometric albedo curves to verify agreement.

As pointed out by Taylor and Coust enis (1998), for the past seventeen years Khare *et al.*'s (1984) data were the only optical

TABLE II
Calculated Refractive Index (n) and Extinction Coefficient (k) Values of Titan's Aerosol Analogues Produced after Irradiation of a Simulated Titan Atmosphere ($N_2 : CH_4$; 98 : 2) by a Cold Plasma Discharge at 2 mbar Pressure and at Room Temperature

Wavelength (nm)	n	Δn	Wavelength (nm)	k	Δk
199.5	1.6805	0.0204	200	0.0197	0.0075
204.5	1.6671	0.0135	205	0.0202	0.0076
209.5	1.6600	0.0122	210	0.0207	0.0078
214.5	1.6537	0.0153	215	0.0212	0.0080
219.5	1.6515	0.0143	220	0.0217	0.0082
224.5	1.6490	0.0136	225	0.0222	0.0084
229.5	1.6463	0.0125	230	0.0227	0.0086
234.5	1.6436	0.0113	235	0.0232	0.0088
239.5	1.6411	0.0093	240	0.0238	0.0090
244.5	1.6380	0.0088	245	0.0243	0.0092
249.5	1.6354	0.0070	250	0.0248	0.0094
254.5	1.6329	0.0058	255	0.0253	0.0096
259.5	1.6306	0.0043	260	0.0258	0.0098
264.5	1.6284	0.0035	265	0.0263	0.0100
269.5	1.6265	0.0022	270	0.0268	0.0102
274.5	1.6246	0.0018	275	0.0273	0.0104
279.5	1.6229	0.0020	280	0.0278	0.0105
284.5	1.6211	0.0029	285	0.0281	0.0107
289.5	1.6196	0.0034	290	0.0285	0.0108
294.5	1.6180	0.0042	295	0.0287	0.0109
299.5	1.6165	0.0047	300	0.0287	0.0109
304.5	1.6150	0.0054	305	0.0286	0.0109
309.5	1.6137	0.0057	310	0.0283	0.0107
314.5	1.6123	0.0063	315	0.0278	0.0105
319.5	1.6111	0.0065	320	0.0271	0.0103
324.5	1.6100	0.0069	325	0.0262	0.0099
329.5	1.6090	0.0071	330	0.0253	0.0096
334.5	1.6080	0.0072	335	0.0242	0.0092
339.5	1.6072	0.0072	340	0.0231	0.0088
344.5	1.6064	0.0073	345	0.0220	0.0083
349.5	1.6056	0.0073	350	0.0208	0.0079
354.5	1.6048	0.0073	355	0.0197	0.0075
359.5	1.6040	0.0075	360	0.0186	0.0071
364.5	1.6032	0.0076	365	0.0175	0.0066
369.5	1.6024	0.0078	370	0.0165	0.0063
374.5	1.6015	0.0080	375	0.0155	0.0059
379.5	1.6006	0.0083	380	0.0146	0.0055
384.5	1.5996	0.0086	385	0.0137	0.0052
389.5	1.5986	0.0091	390	0.0128	0.0049
394.5	1.5975	0.0096	395	0.0120	0.0046
399.5	1.5964	0.0102	400	0.0113	0.0043
404.5	1.5952	0.0107	405	0.0106	0.0040
409.5	1.5939	0.0115	410	0.0099	0.0038
414.5	1.5926	0.0122	415	0.0093	0.0035
419.5	1.5912	0.0130	420	0.0087	0.0033
424.5	1.5898	0.0139	425	0.0082	0.0031
429.5	1.5884	0.0148	430	0.0077	0.0029
434.5	1.5869	0.0157	435	0.0072	0.0027
439.5	1.5854	0.0166	440	0.0068	0.0026
444.5	1.5839	0.0175	445	0.0064	0.0024
449.5	1.5825	0.0184	450	0.0060	0.0023
454.5	1.5811	0.0193	455	0.0056	0.0021
459.5	1.5798	0.0201	460	0.0053	0.0020
464.5	1.5784	0.0209	465	0.0050	0.0019
469.5	1.5771	0.0217	470	0.0047	0.0018

TABLE II—Continued

Wavelength (nm)	n	Δn	Wavelength (nm)	k	Δk
474.5	1.5758	0.0226	475	0.0045	0.0017
479.5	1.5746	0.0233	480	0.0042	0.0016
484.5	1.5734	0.0240	485	0.0040	0.0015
489.5	1.5726	0.0244	490	0.0038	0.0014
494.5	1.5719	0.0246	495	0.0036	0.0014
499.5	1.5716	0.0246	500	0.0034	0.0013
504.5	1.5714	0.0245	505	0.0032	0.0012
509.5	1.5711	0.0244	510	0.0031	0.0012
514.5	1.5708	0.0245	515	0.0029	0.0011
519.5	1.5704	0.0245	520	0.0028	0.0010
524.5	1.5699	0.0247	525	0.0026	0.0010
529.5	1.5693	0.0251	530	0.0025	0.0009
532.5	1.5692	0.0251	535	0.0024	0.0009
537.5	1.5691	0.0251	540	0.0023	0.0009
542.5	1.5688	0.0250	545	0.0021	0.0008
547.5	1.5685	0.0252	550	0.0020	0.0008
552.5	1.5681	0.0252	555	0.0020	0.0007
557.5	1.5677	0.0254	560	0.0019	0.0007
562.5	1.5673	0.0254	565	0.0018	0.0007
567.5	1.5669	0.0257	570	0.0017	0.0006
572.5	1.5664	0.0257	575	0.0016	0.0006
577.5	1.5660	0.0259	580	0.0016	0.0006
582.5	1.5655	0.0258	585	0.0015	0.0006
587.5	1.5653	0.0257	590	0.0014	0.0005
592.5	1.5650	0.0254	595	0.0014	0.0005
597.5	1.5648	0.0255	600	0.0013	0.0005
602.5	1.5644	0.0252	605	0.0013	0.0005
607.5	1.5639	0.0250	610	0.0012	0.0005
612.5	1.5629	0.0240	615	0.0012	0.0004
617.5	1.5613	0.0226	620	0.0011	0.0004
622.5	1.5600	0.0217	625	0.0011	0.0004
627.5	1.5592	0.0218	630	0.0011	0.0004
632.5	1.5584	0.0211	635	0.0010	0.0004
637.5	1.5578	0.0211	640	0.0010	0.0004
642.5	1.5571	0.0205	645	0.0010	0.0004
647.5	1.5566	0.0203	650	0.0009	0.0004
652.5	1.5561	0.0196	655	0.0009	0.0003
657.5	1.5553	0.0186	660	0.0009	0.0003
662.5	1.5543	0.0176	665	0.0009	0.0003
667.5	1.5533	0.0166	670	0.0008	0.0003
672.5	1.5527	0.0165	675	0.0008	0.0003
677.5	1.5520	0.0158	680	0.0008	0.0003
682.5	1.5515	0.0157	685	0.0008	0.0003
687.5	1.5509	0.0151	690	0.0007	0.0003
692.5	1.5504	0.0150	695	0.0007	0.0003
697.5	1.5497	0.0143	700	0.0007	0.0003
702.5	1.5493	0.0143	705	0.0007	0.0003
707.5	1.5487	0.0136	710	0.0007	0.0003
712.5	1.5482	0.0136	715	0.0007	0.0003
717.5	1.5475	0.0129	720	0.0007	0.0003
722.5	1.5470	0.0129	725	0.0006	0.0002
727.5	1.5464	0.0123	730	0.0006	0.0002
732.5	1.5459	0.0123	735	0.0006	0.0002
737.5	1.5454	0.0117	740	0.0006	0.0002
742.5	1.5449	0.0117	745	0.0006	0.0002
747.5	1.5443	0.0112	750	0.0006	0.0002
752.5	1.5438	0.0112	755	0.0006	0.0002
757.5	1.5432	0.0106	760	0.0006	0.0002
762.5	1.5429	0.0105	765	0.0006	0.0002

TABLE II—Continued

Wavelength (nm)	n	Δn	Wavelength (nm)	k	Δk
767.5	1.5424	0.0100	770	0.0006	0.0002
772.5	1.5420	0.0100	775	0.0006	0.0002
777.5	1.5414	0.0095	780	0.0006	0.0002
782.5	1.5410	0.0095	785	0.0006	0.0002
787.5	1.5405	0.0090	790	0.0006	0.0002
792.5	1.5402	0.0089	795	0.0006	0.0002
797.5	1.5397	0.0084	800	0.0006	0.0002
802.5	1.5394	0.0083	805	0.0006	0.0002
807.5	1.5389	0.0077	810	0.0006	0.0002
812.5	1.5387	0.0076	815	0.0006	0.0002
817.5	1.5383	0.0071	820	0.0005	0.0002
822.5	1.5380	0.0069	825	0.0005	0.0002
827.5	1.5377	0.0064	830	0.0005	0.0002
832.5	1.5374	0.0063	835	0.0005	0.0002
837.5	1.5371	0.0057	840	0.0005	0.0002
842.5	1.5368	0.0057	845	0.0005	0.0002
847.5	1.5364	0.0052	850	0.0005	0.0002
853	1.5362	0.0051	855	0.0005	0.0002
858	1.5358	0.0047	860	0.0004	0.0002
863	1.5355	0.0046	865	0.0004	0.0002
868	1.5352	0.0042	870	0.0004	0.0002
873	1.5349	0.0041	875	0.0004	0.0002
878	1.5346	0.0036	880	0.0004	0.0002
883	1.5343	0.0036	885	0.0004	0.0002
888	1.5340	0.0032	890	0.0004	0.0001
893	1.5338	0.0031	895	0.0004	0.0001
898	1.5336	0.0027	900	0.0004	0.0001
903	1.5334	0.0026	905	0.0004	0.0001
908	1.5331	0.0023	910	0.0004	0.0001
913	1.5330	0.0022	915	0.0004	0.0001
918	1.5327	0.0019	920	0.0004	0.0001
923	1.5325	0.0018	925	0.0003	0.0001
928	1.5323	0.0016	930	0.0003	0.0001
933	1.5322	0.0015	935	0.0003	0.0001
938	1.5320	0.0012	940	0.0003	0.0001
943	1.5318	0.0012	945	0.0003	0.0001
948	1.5317	0.0009	950	0.0003	0.0001
953	1.5316	0.0008	955	0.0003	0.0001
958	1.5314	0.0005	960	0.0003	0.0001
963	1.5314	0.0004	965	0.0003	0.0001
968	1.5313	0.0001	970	0.0003	0.0001
973	1.5313	0.0002	975	0.0003	0.0001
978	1.5312	0.0003	980	0.0003	0.0001
983	1.5312	0.0006	985	0.0003	0.0001
988	1.5311	0.0007	990	0.0003	0.0001
993	1.5311	0.0010	995	0.0003	0.0001
998	1.5310	0.0096	1000	0.0003	0.0001

Note. Δn and Δk numbers correspond to absolute limits. They are calculated from the variation in the n and k values obtained after considering the effect of the thickness uncertainty and the amount of light scattered by the two samples (2H and 4H).

constants available to be used in radiative transfer studies of Titan's haze and have remained as the "typical" laboratory reference. We expect that the data of the present work will be particularly useful for explaining Titan's albedo behavior, specifically the flat appearance observed in the UV domain. They can

also help to clarify the nature of the dark and bright regions observed on Titan's surface. According to Griffith *et al.* (1991) and Smith *et al.* (1996) calculated albedos of Titan's surface are consistent with a surface in which regions of water ice or weathered high terrain can be differentiated from dark material. Possible candidates for the dark material are ethane–methane lakes or sediments of organic solids with a low reflectivity. Our aerosol analogues display a monotonic reflectance value of 0.07 for wavelengths longer than 700 nm, and exhibit reflectance values as low as 0.03 around 450 nm, as shown in Fig. 2b. If one assumes that this reflectance value is low enough and geologic time has allowed the formation of a thin aerosol coating, our aerosol analogues can qualify as an appropriate material for explaining the presence of dark features on Titan's surface. Our results can also contribute to the interpretation of the data collected by the different scientific instruments onboard the Cassini-Huygens spacecraft such as the DISR (descent imager/spectral radiometer), the ACP (aerosol collector and pyrolyzer), the UVIS (ultraviolet imaging spectrograph), and the VIMS (visible and infrared mapping spectrometer). Among the many scientific objectives of these instruments are the determination of the satellite's atmospheric composition and the study of the physical, chemical, and optical properties of the aerosols. Current work is being developed to extend the calculations of n and k to the 0.9–2.5 μm range. These measurements will be useful in constraining the observations of Titan's surface through some of the methane windows, mainly present in the IR domain. Values of the optical constants of the aerosols and ices expected to exist on Titan's surface will be needed to constrain all the data received from the Cassini-Huygens mission.

APPENDIX

Formulas used in the incoherent treatment of transmittance and reflectance data (Abelès, 1967):

$$R = [a.b.d^{2k\eta} + a.c.d^{-2k\eta} + 2.r.\cos(2.n.\eta) + 2.s.\sin(2.n.\eta)]/D$$

$$T = [16.n_o.n_s(n^2 + k^2)]/D$$

where:

$$D = b.e.d^{2k\eta} + a.c.d^{-2k\eta} + 2.t.\cos(2.n.\eta) + 2.u.\sin(2.n.\eta)$$

$$a = (n - n_o)^2 + k^2$$

$$b = (n + n_s)^2 + k^2$$

$$c = (n - n_s)^2 + k^2$$

$$e = (n + n_o)^2 + k^2$$

$$r = (n_o^2 + n_s^2)(n^2 + k^2) - n_o n_s k^2 - (n^2 + k^2)^2$$

$$t = (n_o^2 + n_s^2)(n^2 + k^2) - n_o n_s k^2 + 4n_o n_s k^2 - (n^2 + k^2)^2$$

$$s = 2.k.(n_s - n_o)(n^2 + k^2 + n_o n_s)$$

$$u = 2.k.(n_s + n_o)(n^2 + k^2 - n_o n_s)$$

$$\eta = 2.\pi.d/\lambda$$

k = extinction coefficient

n = refractive index

n_o = incident medium refractive index

n_s = substrate refractive index

d = aerosol film thickness

λ = wavelength

ACKNOWLEDGMENTS

This work was supported by ECOS/CONACyT-SEP-ANNUIES in the frame of the action number M97U01 and also by grants from CNES (IDS Cassini-Huygens mission program). The authors express their gratitude to Christine Andraud (Laboratoire d'Optique des Solides, Université Paris 6) for her deep involvement in optical measurements and to Patrick Dreyfus (CHU Henri Mondor, Créteil) for providing facilities for doing confocal microscopy measurements. We also wish to thank Bishun N. Khare and Ralph Lorenz for their detailed review of the initial manuscript and their valuable comments. This paper also benefited from discussions with Raj K. Khanna.

REFERENCES

- Abelès, F. 1967. Optics of thin films. In *Advanced Optical Techniques* (A. C. S. Van Heel, Ed.), pp. 143–188. Wiley, New York, North Holland, Amsterdam.
- Atreya, S. K. 1986. *Atmospheres and Ionospheres of the Outer Planets*. Springer-Verlag, New York.
- Chang, J.-S., P. A. Lawless, and T. Yamamoto 1991. Corona discharge processes. *IEEE Trans. Plasma Sci.* **19**, 1152–1166.
- Coll, P., D. Coscia, M.-C. Gazeau, L. Guez, and F. Raulin 1998. Review and latest results of laboratory investigations of Titan's aerosols. *Origins Life Evol. Biosph.* **28**, 195–213.
- Coll P., D. Coscia, N. Smith, M.-C. Gazeau, S. I. Ramírez, G. Cernogora, G. Israël, and F. Raulin 1999. Experimental laboratory simulation of Titan's atmosphere (aerosols and gas phase). *Planet. Space Sci.* **47**, 1331–1340.
- Courtin, R., D. Gautier, and C. P. McKay 1995. Titan's thermal emission spectrum: Reanalysis of the Voyager infrared measurements. *Icarus* **114**, 144–162.
- Cousténis, A., E. Lellouch, J. P. Maillard, and C. P. McKay 1995. Titan's surface: Composition and variability from the near-infrared albedo. *Icarus* **118**, 87–104.
- Danielson, R. E., J. J. Caldwell, and D. R. Larach 1973. An inversion in the atmosphere of Titan. *Icarus* **20**, 437–443.
- de Vanssay, E., G. D. McDonald, and B. N. Khare 1999. Evidence from scanning electron microscopy of experimental influences on the morphology of Triton and Titan tholins. *Planet. Space Sci.* **47**, 433–440.
- Demichelis, F., G. Kaniadakis, A. Tagliaferro, and E. Tresso 1987. New approach to optical analysis of absorbing thin solid films. *Appl. Opt.* **26**, 1737–1740.
- Griffith, C. A., T. Owen, and R. Wagener 1991. Titan's surface and troposphere, investigated with ground-based, near-infrared observations. *Icarus* **93**, 362–378.
- Grigorovici, R., T. Stoica, and A. Vancu 1982. Evaluation of the optical constants and thicknesses of weakly absorbing non-uniform tin films. *Thin Solid Films* **97**, 173–185.
- Hunten, D. M., G. Tomasko, F. M. Flasar, R. E. Samuelson, D. F. Strobel, and D. J. Stevenson 1984. Titan. In *Saturn* (T. Gehrels and M. S. Matthews, Eds.), pp. 671–759. Univ. of Arizona Press, Tucson.
- Khare, B. N., C. Sagan, E. T. Arakawa, F. Suits, T. A. Callcott, and M. W. Williams 1984. Optical constants of organic tholins produced in a simulated titanian atmosphere: From soft X-ray to microwave frequencies. *Icarus* **60**, 127–137.
- Khare, B. N., C. Sagan, W. R. Thompson, E. T. Arakawa, and P. Votaw 1987. Solid hydrocarbon aerosols produced in simulated uranian and neptunian stratospheres. *J. Geophys. Res.* **92**, 15067–15082.
- Kouvaris, L. C., and F. M. Flasar 1991. Phase equilibrium of methane and nitrogen at low temperatures: Application to Titan. *Icarus* **91**, 112–124.
- Lellouch, E., A. Cousténis, D. Gautier, F. Raulin, N. Dubouloz, and C. Frère 1989. Titan's atmosphere and hypothesized ocean: A reanalysis of the Voyager I radio-occultation and IRIS 7.7 μm data. *Icarus* **79**, 328–349.

- Lorenz, R. D., M. T. Lemmon, P. H. Smith, and G. W. Lockwood 1999. Seasonal change on Titan observed with the Hubble Space Telescope WFPC-2. *Icarus* **142**, 391–401.
- Maxwell-Garnett, J. C. 1904. Colours in metal glasses and in metallic films. *Philos. Trans. R. Soc. London* **203**, 385–420.
- McKay, C. P. 1996. Elemental composition, solubility and optical properties of Titan's organic haze. *Planet. Space Sci.* **44**, 741–747.
- McKay, C. P., and O. B. Toon 1992. Titan's organic haze. In *Proceedings of the Symposium on Titan*, ESA SP-338, pp. 185–190. European Space Agency, Noordwijk, The Netherlands.
- McKay, C. P., J. B. Pollack, and R. Courtin 1989. The thermal structure of Titan's atmosphere. *Icarus* **80**, 23–53.
- McKay, C. P., J. B. Pollack, and R. Courtin 1991. The greenhouse and anti-greenhouse effects on Titan. *Science* **253**, 1118–1121.
- Morrison, D., T. Owen, and L. A. Soderblom 1986. The satellites of Saturn. In *Satellites* (J. A. Burns and M. S. Matthews, Eds.), pp. 764–801. Univ. Arizona Press, Tucson.
- Neff, J. S., D. C. Humm, J. T. Bergstralh, A. L. Cochran, W. D. Cochran, E. S. Barker, and R. G. Tull 1984. Absolute spectrophotometry of Titan, Uranus, and Neptune: 3500–10,500 Å. *Icarus* **60**, 221–235.
- Rages, K., and J. B. Pollack 1980. Titan's aerosols: Optical properties and vertical distribution. *Icarus* **41**, 119–130.
- Rannou, P., M. Cabane, E. Chassefière, R. Botet, C. P. McKay, and R. Courtin 1995. Titan's geometric albedo: Role of the fractal structure of the aerosols. *Icarus* **118**, 355–372.
- Sagan, C., and W. R. Thompson 1984. Production and condensation of organic gases in the atmosphere of Titan. *Icarus* **59**, 133–161.
- Sagan, C., B. N. Khare, and J. S. Lewis 1984. Organic matter in the Saturn system. In *Saturn* (T. Gehrels and M. S. Matthews, Eds.), pp. 788–807. Univ. Arizona Press, Tucson.
- Samuelson, R. E. 1983. Radiative equilibrium model of Titan's atmosphere. *Icarus* **53**, 364–387.
- Samuelson, R. E., and L. A. Mayo 1991. Thermal infrared properties of Titan's stratospheric aerosol. *Icarus* **91**, 207–219.
- Scattergood, T. W., C. P. McKay, J. B. Pollack, and C. R. Giver 1988. Titan's organic haze over the last four billion years. *Bull. Am. Astron. Soc.* **20**, 842.
- Scattergood, T. W., C. P. McKay, W. J. Borucki, L. P. Giver, H. Van Ghyseghe, J. E. Parris, and S. L. Miller 1989. Production of organic compounds in plasmas: A comparison among electric sparks, laser-induced plasmas, and UV light. *Icarus* **81**, 413–428.
- Smith, P. H., M. T. Lemmon, R. D. Lorenz, L. A. Sromovsky, J. J. Caldwell, and M. D. Allison 1996. Titan's surface revealed by HST imaging. *Icarus* **119**, 336–349.
- Strobel, D. F., D. T. Hall, X. Zhu, and M. F. Summers 1993. Upper limit on Titan's atmospheric argon abundance. *Icarus* **103**, 333–336.
- Swanepoel, R. 1984. Determination of surface roughness and optical constants of inhomogeneous amorphous silicon films. *J. Phys. E: Sci. Instrum.* **17**, 896–903.
- Taylor, F. W., and A. Cousténis 1998. Titan in the Solar System. *Planet. Space Sci.* **46**, 1085–1097.
- Thompson, W. R., T. J. Henry, J. M. Schwartz, B. N. Khare, and C. Sagan 1991. Plasma discharge in N₂ + CH₄ at low pressures: Experimental results and applications to Titan. *Icarus* **90**, 57–73.
- Toon, O. B., C. P. McKay, C. A. Griffith, and R. P. Turco 1992. A physical model of Titan's aerosols. *Icarus* **95**, 24–53.